GEOLOGY | THE GEOLOGICAL SOCIETY OF AMERICA®

https://doi.org/10.1130/G47280.1

Manuscript received 30 November 2019
Revised manuscript received 9 March 2020
Manuscript accepted 12 March 2020

Diverse rock types detected in the lunar South Pole–Aitken Basin by the Chang'E-4 lunar mission

Jun Huang (黄俊)[1,2*] Zhiyong Xiao (肖智勇)[2,3,4*] Long Xiao (肖龙)[1,2,4*] Briony Horgan[5], Xiaoyi Hu (胡晓依)[1], Paul Lucey[6], Xiao Xiao (肖潇)[1] Siyuan Zhao (赵思源)[1] Yuqi Qian (钱煜奇)[1] Hao Zhang (张昊)[1] Chunlai Li (李春来)[7] Rui Xu (徐睿)[7] Zhiping He (何志平)[7] Jianfeng Yang (杨建峰)[8] Bin Xue (薛彬)[8] Qi He (何琦)[1] Jie Zhong (钟杰)[9] Hongyu Lin (林宏宇)[10] Changning Huang (黄长宁)[10] Jianfeng Xie (谢剑锋)[11]

[1]State Key Laboratory of Geological Processes and Mineral Resources, Planetary Science Institute, School of Earth Sciences, China University of Geosciences, Wuhan, Hubei 430074, China
[2]Chinese Academy of Sciences (CAS) Center for Excellence in Comparative Planetology, Hefei, Anhui 230026, China
[3]Planetary Environmental and Astrobiological Laboratory, School of Atmospheric Sciences, Sun Yat-sen University, Zhuhai, Guangdong 519000, China
[4]State Key Laboratory of Lunar and Planetary Sciences, Space Science Institute, Macau University of Science and Technology, Macau 999078, China
[5]Department of Earth, Atmospheric and Planetary Sciences, Purdue University, West Lafayette, Indiana 47907, USA
[6]Hawai'i Institute of Geophysics and Planetology, University of Hawai'i at Manoa, Honolulu, Hawai'i 96822, USA
[7]Key Laboratory of Space Active Opto-Electronics Technology, Shanghai Institute of Technical Physics, Chinese Academy of Sciences, Shanghai 200083, China
[8]Xi'an Institute of Optics and Precision Mechanics, Chinese Academy of Sciences, Xi'an, 710119, China
[9]Institute of Optics and Electronics, Chinese Academy of Sciences, Chengdu 610209, China
[10]Institute of Space Mechanics and Electricity, China Academy of Space Technology, Beijing 100086, China
[11]Beijing Aerospace Flight Control Center, Beijing 100094, China

ABSTRACT

The South Pole–Aitken (SPA) basin, located between the South Pole and Aitken crater on the far side of the Moon, is the largest confirmed lunar impact structure. The pre-Nectarian SPA basin is a 2400 × 2050 km elliptical structure centered at 53°S, 191°E, which should have exposed lower crust and upper mantle due to the enormous excavation depth. Olivine, the dominant mineral in Earth's mantle, has only been identified in small and localized exposures in the margins of the SPA basin, and the dominant mafic component is, instead, pyroxene. These mineralogical characteristics could be explained by the recent hypothesis that the lunar upper mantle is dominated by low-calcium pyroxene, not olivine. Here, we present observations from imaging and spectral data from China's Chang'E-4 (CE-4) lunar mission in the first 4 synodic days, especially the first *in situ* visible/near-infrared spectrometer observations of an exposed boulder. We identified a variety of rock types, but not the recently reported olivine-rich materials in the landing region. The results are consistent with orbital observations. The obtained mineralogical information provides a better understanding of the nature and origin of SPA materials.

INTRODUCTION

The surface materials of the South Pole–Aitken (SPA) basin show distinct chemical (Lucey et al., 1998; Jolliff et al., 2000) and mineralogical (Pieters et al., 2001; Ohtake et al., 2014; Moriarty and Pieters, 2018) characteristics compared to other compositional regions on the Moon. The vast scale of the SPA basin-forming event is modeled as having produced a thick ejecta blanket, which excavated materials from throughout the crust and down into the upper mantle (Melosh et al., 2017). However, orbital studies of SPA basin have revealed very few exposures of Earth-like olivine-rich mantle material (Yamamoto et al., 2012), and they instead show abundant low-calcium pyroxene (LCP; Melosh et al., 2017; Moriarty and Pieters, 2018) and some high-calcium pyroxene (HCP; Ohtake et al., 2014; Moriarty et al., 2019). SPA also should have generated thick impact melt, which has been hypothesized to have undergone igneous differentiation (Morrison, 1998; Nakamura et al., 2009; Hurwitz and Kring, 2014; Vaughan and Head, 2014). Modeling has indicated that the approximate diameter of the differentiated melt sheet is ~400 km (Hurwitz and Kring, 2014), which is roughly spatially consistent with the South Pole–Aitken compositional anomaly (SPACA; Moriarty and Pieters, 2018), a central HCP-dominated spectral unit (Fig. 1A) with distinctive topographic and slope properties compared to the rest of the SPA basin (Ohtake et al., 2014). Assuming an olivine-rich upper mantle, a possible top-to-bottom compositional stratigraphy of the differentiated melt is norite, pyroxenite, and dunite (Hurwitz and Kring, 2014; Vaughan and Head, 2014).

The Chang'E-4 (CE-4) lunar spacecraft mission (Chinese Lunar Exploration Program) was planned to provide *in situ* observations to address the fundamental question about the possible results of SPA melt differentiation and the composition of the lunar upper mantle (Huang

*E-mails: junhuang@cug.edu.cn; xiaozhiyong@mail.sysu.edu.cn; longxiao@cug.edu.cn.

CITATION: Huang, J., et al., 2020, Diverse rock types detected in the lunar South Pole–Aitken Basin by the Chang'E-4 lunar mission: Geology, v. 48, p. , https://doi.org/10.1130/G47280.1

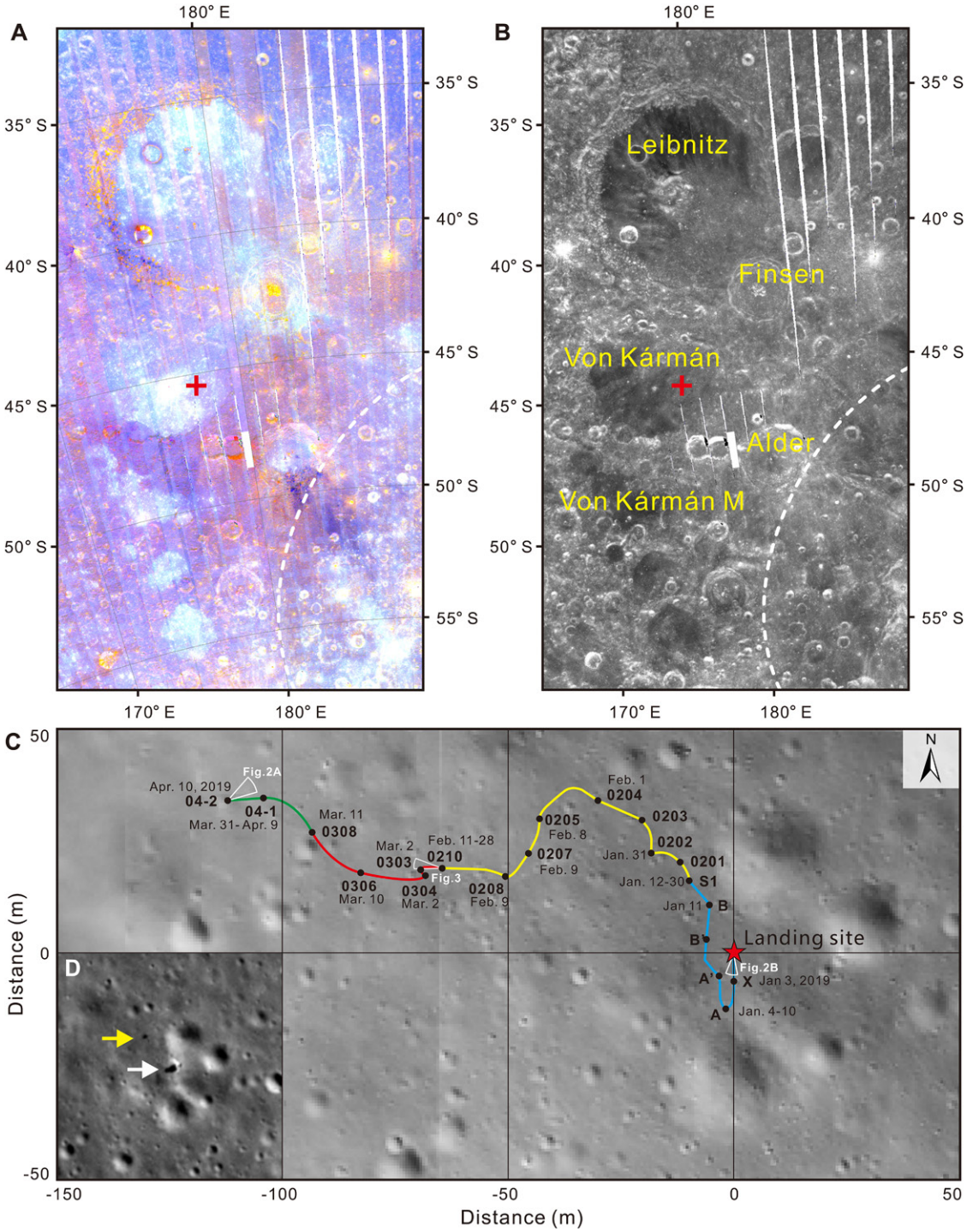

Figure 1. Geologic context of the Chang'E-4 (CE-4) lunar spacecraft mission (Chinese Lunar Exploration Program) landing region and *in situ* exploration traverse route of rover Yutu-2. (A) Multispectral Imager (MI) color composite mosaic of the Von Kármán region; continuum-removed reflectance spectra of bands at 900 nm, 1050 nm, and 1250 nm are assigned to red, green, and blue channels, respectively. CE-4 landing point is marked with red cross. (B) MI mosaic of 750 nm reflectance. Von Kármán M, Von Kármán, Alder, Finsen, and Leibnitz craters are labeled in yellow. White dashed line is part of outer margins of hypothesized South Pole–Aitken (SPA) impact melt pond (Ohtake et al., 2014). (C) Traverse of Yutu-2 in first 4 synodic days on landing camera (LCAM) mosaic. Blue, yellow, red, and green lines indicate traverse of synodic day 1, 2, 3, and 4, respectively. Letters and numbers besides black dots are names of navigation points. Red star marks landing point. (D) NASA Lunar Reconnaissance Orbiter Narrow Angle Camera (NAC) image for lander (yellow arrow) and Yutu-2 (white arrow).

et al., 2018). With the help of a relay satellite (Que Qiao) at the Earth-Sun Lagrangian 2 point (1.5×10^6 km directly 'behind' Earth as viewed from the Sun), the CE-4 lander and the rover (Yutu-2) have been conducting successful exploration of the lunar far side for the first time (Wu et al., 2019). The landing site is located in a relatively high-albedo region within Von Kármán crater (Fig. 1B), which can be tracked as LCP-bearing ejecta from Finsen crater, based on orbital reflectance spectra data (Huang et al., 2018). Yutu-2 traveled 178.9 m in the first 4 synodic days, and 24 observations were made by the visible/near-infrared spectrometer (VNIS) along the route (Fig. 1C), of which 18 were analyzed here. Here, we report diverse rock types using the VNIS data and the panorama camera (PCAM) on Yutu-2 and the landing camera (LCAM) and the terrain camera (TCAM) on the lander.

IMAGING RESULTS

The stratigraphic framework of the landing area features a surface layer dominated by the ejecta deposits from Finsen crater and other various-aged nearby craters and the underlying mare basalts (Huang et al., 2018). Images obtained by the LCAM and PCAM show that the landing region is relatively free of large boulders (>1 m), indicating a relatively long time of degradation, which is consistent with the estimated thicknesses of regolith and impact crater ejecta (Huang et al., 2018). Craters with diameters of centimeters to tens of meters (Figs. 1C and 2A) were observed. We also identified clusters of centimeter-size rock fragments in the rover exploration region (Fig. 2A), which are most likely shattered clusters of ejecta launched from other impact craters

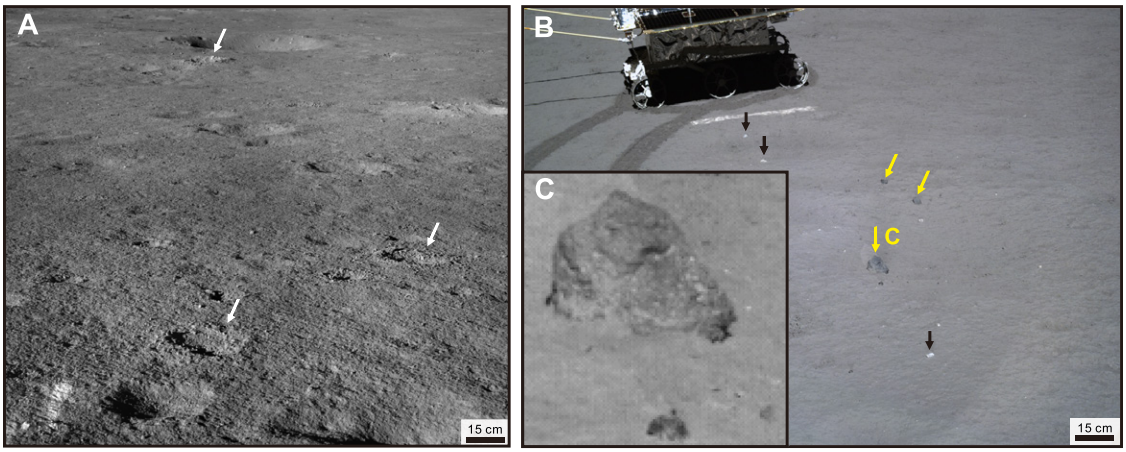

Figure 2. Panorama camera (PCAM) and terrain camera (TCAM) observations in the Chang'E-4 (CE-4) landing region. (A) Craters with different sizes. Clusters of rock fragments (white arrows) were frequently identified. (B) Relatively dark-toned (yellow arrows) and light-toned (black arrows) rocks. (C) Close-up view of dark-toned rock. Light-toned spots are plagioclase phenocrysts or pits created by micrometeorite impacts.

(Schultz and Gault, 1985). Similar occurrences of pebble-decorated small and shallow craters were also observed near the NASA Surveyor 7 landing site (Shoemaker et al., 1969). A few rocks around the lander exhibit lighter or darker tones compared to the regolith and most other surface rocks (Fig. 2B), where the relatively light-toned rocks resemble feldspar-rich rocks (e.g., anorthosite), and the relatively dark rocks resemble mafic-mineral–dominated lunar rocks (e.g., basalt) or meteorites. Unfortunately, the Yutu-2 did not perform VNIS observations of these interesting targets.

The PCAM instrument observed a group of relatively light-toned rocks near a local depression (Fig. 3A). One of the rocks, which we informally name as "Qi Yuan" ("unexpected encounter" in Chinese), is ~15–20 cm in size, with an irregular shape. Qi Yuan looks like a coherent igneous rock, and the bright spots on its relatively fresh surface are possibly either plagioclase phenocrysts or pits created by micrometeorite impacts (Fig. 3B). However, we cannot rule out a breccia origin due to the limited resolution of the image. The VNIS instrument made four attempts to take a spectrum of Qi Yuan, of which only the fourth was successful (Fig. 3C). It is the first *in situ* visible/near-infrared spectrum of a lunar rock (Fig. 4A).

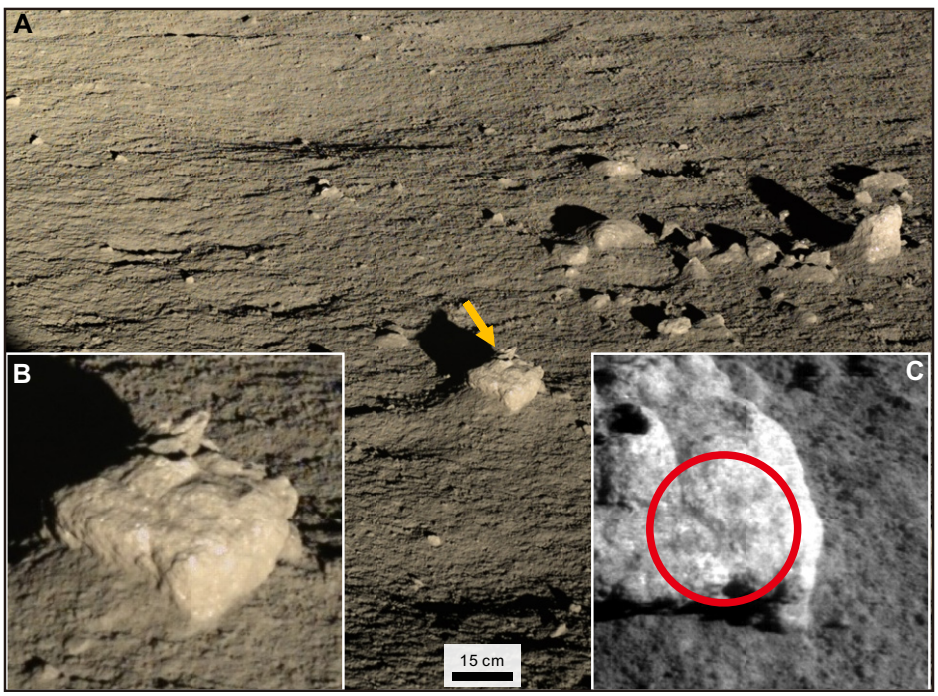

Figure 3. Panorama camera (PCAM) and visible/near-infrared spectrometer (VNIS) observations of Qi Yuan—the first lunar rock for which a VNIS spectrum was obtained. (A) Group of relatively light-toned rocks. Half-buried rocks were likely exposed due to long-term mass wasting. Qi Yuan is indicated by yellow arrow. (B) Close-up view of Qi Yuan, which looks like a coherent igneous rock; bright spots on its relatively fresh surface are plagioclase phenocrysts or pits created by micrometeorite impacts. (C) VNIS visible image of Qi Yuan. Red circle indicates footprint of VNIS short-wave infrared detector.

IN SITU SPECTROSCOPY RESULTS

The spectrum of Qi Yuan shows more prominent 1 μm and 2 μm spectral features (Fig. S1A in the Supplemental Material[1]) than those of the regolith (Fig. 4A), but all of the VNIS-obtained spectra exhibit red slopes due to space weathering (Pieters et al., 2000; Hapke, 2001). The spectral features around 1 μm and 2 μm are due to an Fe^{2+} crystal field absorption (Burns, 1993), and the center position and shape of the 1 and 2 μm bands are diagnostic of mafic mineralogy and composition (Adams, 1968). We removed the continuum of Qi Yuan's spectrum by fitting a second-order polynomial convex hull to tie points adjusted to the maximize band area near 0.7, 1.5, and 2.35 μm. The continuum-removed spectrum of Qi Yuan (Fig. S1B) exhibits a 1 μm band centered near 0.96 μm, and a 2 μm band centered near 2.03 μm (Fig. S2B). The 1 μm band is slightly asymmetric, with 18% more band area at longer wavelengths. These values are consistent with laboratory spectra of intermediate pyroxenes like pigeonite or mixtures of orthopyroxene and clinopyroxene (Cloutis and Gaffey, 1991; Klima et al., 2007, 2011; Horgan et al., 2014; Moriarty and Pieters, 2016; Viviano et al., 2019), and the moderate asymmetry suggests limited spectral contribution from olivine, glass, or feldspar absorptions centered between 1.15 and 1.3 μm (Horgan et al., 2014). This observation seems at odds with the fact that the 1 μm band is more than 4 times deeper than the 2 μm band, which would normally indicate significant olivine. However, the position and low asymmetry of the 1 μm band do not support significant contribution from olivine. The VNIS spectrum exhibits a much higher 1 μm and 2 μm band area ratio compared to both NASA Apollo samples, which showed similar 1 μm band centers and regional orbital spectra (Figs. S2C and

[1]Supplemental Material. Supplemental information and figures. Please visit https://doi.org/10.1130/GEOL.26213S.12114414 to access the supplemental material, and contact editing@geosociety.org with any questions.

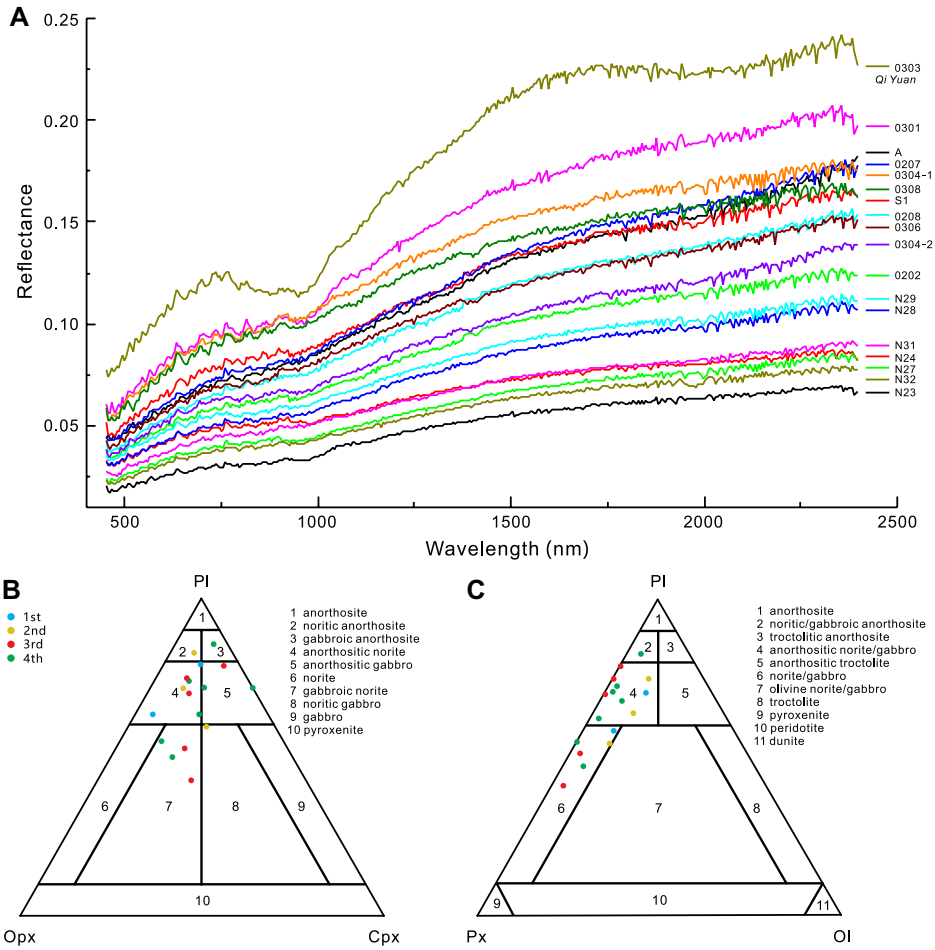

Figure 4. Visible/near-infrared spectrometer (VNIS)–obtained spectra and look-up table (LUT) mineral abundance of lunar regolith. (A) Spectra of all VNIS observations in first 4 synodic days. (B) LUT mineral abundances on orthopyroxene-clinopyroxene-plagioclase (Opx-Cpx-Pl) ternary diagram. (C) LUT mineral abundances on pyroxene-olivine-plagioclase (Px-Ol-Pl) ternary diagram.

S2F), suggesting that the spectrum is anomalous compared to other lunar spectra. Thus, it may be more likely that the 2 μm band is weak due to the low signal detected by the spectrometer in this range.

Instead, the slight asymmetry in the 1 μm band is more likely due to significant feldspar (Cheek and Pieters, 2014). In comparison to the spectral properties of Apollo samples (Figs. S2A–S2C), the VNIS spectrum is most like pyroxene and feldspar-dominated mare soils and rocks with very little olivine (<4%), based on their band centers and asymmetries (Fig. S1B). Thus, the spectral properties of Qi Yuan appear to be consistent with a pyroxene and feldspar-dominated assemblage with at most minor olivine, where the pyroxene is composed of either pigeonite or a mixture of clinopyroxene and orthopyroxene.

For all the 17 observation of the lunar regolith in the landing region, we removed the continuum of the spectra by subtracting the connecting line of reflectance values between 750 and 1550 nm. Then, we generated a lunar spectral mineral look-up table (LUT) with 17 μm grain size (Pieters et al., 1993) and Mg number of 65 (Lucey et al., 2014) using a radiative transfer model (Lucey, 2004; Denevi et al., 2008; Lucey et al., 2014) at the wavelength range of 750–1550 nm. Finally, we fit the spectra following the procedures applied to the Chang'E-3 VNIS data (Zhang et al., 2015) to estimate the abundances of plagioclase (Pl), orthopyroxene (Opx), clinopyroxene (Cpx), and olivine (Ol). The method is detailed in the supplementary material. Mineral abundances are the mean values of a comprehensive set of fitting results (Table S1). We did not derive the mineral abundances for Qi Yuan using the LUT method, because this method was constructed using only lunar regolith samples, and it might induce large errors and uncertainties in estimation of mineral abundance due to grain size and/or phase angle effects.

The modeled olivine concentrations of all observations were less than 12%, and we plotted the estimated mineral abundances on two ternary diagrams. In the Px-Ol-Pl (Px—pyroxene) ternary diagram (Fig. 4B), 10 out of 17 VNIS observations fall into the field of anorthositic norite/gabbro for intrusive igneous rocks, which have elevated plagioclase concentrations. Six out of 17 VNIS observations fall into norite/gabbro. Only one observation falls into noritic/gabbroic anorthosite with highest plagioclase concentration. In the Opx-Cpx-Pl ternary diagram (Fig. 4C), we can see most observations have higher Opx concentrations than Cpx. These results are consistent with our interpretation for Qi Yuan based on band parameters above, perhaps suggesting a similar origin for Qi Yuan and at least some of the regolith materials. Interestingly, the 7 VNIS spectra on the fourth synodic day were obtained while Yutu-2 rotated heading without changing its location, so these spectra are all from a very small area. The large compositional variation in an area less than a few square meters is consistent with the idea that the landing region has received multiple sources of various-aged impact ejecta (Huang et al., 2018).

INTERPRETATIONS AND IMPLICATIONS

Various types of rock identified using spectral and imaging data in the landing site are expected from orbital observation (Huang et al., 2018). The dark-toned rocks (Fig. 2B) could originate from the local mare infill excavated by craters penetrating through the overlying ejecta, while the light-toned rocks (Fig. 2B) could have been delivered by craters that impacted the heterogeneous annulus (Moriarty and Pieters, 2018) unit (Fig. 1A). Orbital spectra of the rim and peak of Finsen crater are generally spectrally similar to both VNIS spectra of Qi Yuan and orbital spectra of the landing site (Figs. S1C–S1D, S2D–S2F), which is consistent with an origin for Qi Yuan (and spectrally similar regolith targets nearby) as an ejected block of plagioclase- and pyroxene-rich materials from Finsen crater that has been exposed by mass wasting (Xiao et al., 2013) or a subsequent impact event (Fig. 1D). Alternatively, Qi Yuan could be a shattered ejecta block (Schultz and Gault, 1985) that was delivered by another impact crater in the heterogeneous annulus unit.

The target material of Finsen crater may include both SPA ejecta sourced from the crust and upper mantle (Melosh et al., 2017) as well as SPA impact melts. In addition, the target material has experienced modification by subsequent impact cratering (e.g., the ejecta from Von Kármán and Leibnitz craters). These processes could have led to significant heterogeneity of the target materials for Finsen crater, which is also supported by the compositional variations of the Leibnitz crater rim (Fig. 1A). However, the location of Finsen crater is ~200 km away from the outer margins of the hypothesized SPA impact melt pond (Fig. 1B; Pieters et al., 2000; Hurwitz and Kring, 2014; Ohtake et al., 2014). Therefore, the SPA impact melt should have been negligible in the target lithology where the Finsen impact occurred. In the Multispectral

Imager color composite, the surface materials (Fig. 1A) at the CE-4 landing region are more akin to heterogeneous annulus unit materials. Thus, our interpretation of the pyroxene- and plagioclase-rich CE-4 spectral properties for Qi Yuan and nearby regolith suggests that they may contain a significant amount of highlands crust (e.g., anorthosite) and an SPA ejecta component.

In summary, CE-4 observations provide the first *in situ* characterization of various types of SPA materials. No olivine-rich mantle materials (Li et al., 2019) have been detected so far, and, instead, the only ultramafic component is Opx mixed with highlands-like materials. Rock samples from the local mare infill and mantle-originated materials should be high-priority targets as Yutu-2 continues roving to the west.

ACKNOWLEDGMENTS

This work was supported by the Strategic Priority Research Program of the Chinese Academy of Sciences (grant XDA17010403), the Natural Science Foundation of China (grants 41773061, 41772050, 41830214, 41773063), the China National Space Administration (CNSA) Pre-research Project on Civil Aerospace Technologies (grant D020101), and the Science and Technology Development Fund of Macau (grants 121/2017/A3, 0042/2018/A2). We thank editor Mark Quigley for editorial handling, and Daniel Moriarty, Hap McSween, and an anonymous reviewer for their constructive comments. CNSA Lunar Exploration and Space Program Center and the Chinese Academy of Sciences Lunar and Deep Space Exploration General Department coordinated data access.

REFERENCES CITED

Adams, J.B., 1968, Lunar and Martian surfaces: Petrologic significance of absorption bands in the near-infrared: Science, v. 159, p. 1453–1455.

Burns, R.G., 1993, Mineralogical Applications of Crystal Field Theory: Cambridge, UK, Cambridge University Press, 224 p., https://doi.org/10.1017/CBO9780511524899.

Cheek, L.C., and Pieters, C.M., 2014, Reflectance spectroscopy of plagioclase-dominated mineral mixtures: Implications for characterizing lunar anorthosites remotely: The American Mineralogist, v. 99, p. 1871–1892, https://doi.org/10.2138/am-2014-4785.

Cloutis, E.A., and Gaffey, M.J., 1991, Spectral-compositional variations in the constituent minerals of mafic and ultramafic assemblages and remote sensing implications: Earth, Moon, and Planets, v. 53, p. 11–53, https://doi.org/10.1007/BF00116217.

Denevi, B., Lucey, P., and Sherman, S., 2008, Radiative transfer modeling of near-infrared spectra of lunar mare soils: Theory and measurement: Journal of Geophysical Research: Planets, v. 113, E02003, https://doi.org/10.1029/2007JE002929.

Hapke, B., 2001, Space weathering from Mercury to the asteroid belt: Journal of Geophysical Research: Planets, v. 106, E5, p. 10039–10073, https://doi.org/10.1029/2000JE001338.

Horgan, B.H.N., Cloutis, E.A., Mann, P., and Bell, J.F., 2014, Near-infrared spectra of ferrous mineral mixtures and methods for their identification in planetary surface spectra: Icarus, v. 234, p. 132–154, https://doi.org/10.1016/j.icarus.2014.02.031.

Huang, J., Xiao, Z., Flahaut, J., Martinot, M., Head, J., Xiao, X., Xie, M., and Xiao, L., 2018, Geological characteristics of Von Kármán Crater, northwestern South Pole–Aitken basin: *Chang'E-4* landing site region: Journal of Geophysical Research: Planets, v. 123, p. 1684–1700, https://doi.org/10.1029/2018JE005577.

Hurwitz, D.M., and Kring, D.A., 2014, Differentiation of the South Pole–Aitken basin impact melt sheet: Implications for lunar exploration: Journal of Geophysical Research: Planets, v. 119, p. 1110–1133, https://doi.org/10.1002/2013JE004530.

Jolliff, B.L., Gillis, J.J., Haskin, L.A., Korotev, R.L., and Wieczorek, M.A., 2000, Major lunar crustal terranes: Surface expressions and crust-mantle origins: Journal of Geophysical Research: Planets, v. 105, E2, p. 4197–4216, https://doi.org/10.1029/1999JE001103.

Klima, R.L., Pieters, C.M., and Dyar, M.D., 2007, Spectroscopy of synthetic Mg-Fe pyroxenes I: Spin-allowed and spin-forbidden crystal field bands in the visible and near-infrared: Meteoritics & Planetary Science, v. 42, p. 235–253, https://doi.org/10.1111/j.1945-5100.2007.tb00230.x.

Klima, R.L., Dyar, M.D., and Pieters, C.M., 2011, Near-infrared spectra of clinopyroxenes: Effects of calcium content and crystal structure: Meteoritics & Planetary Science, v. 46, p. 379–395, https://doi.org/10.1111/j.1945-5100.2010.01158.x.

Li, C., Liu, D., Liu, B., Ren, X., Liu, J., He, Z., Zuo, W., Zeng, X., Xu, R., and Tan, X., 2019, *Chang'E-4* initial spectroscopic identification of lunar far-side mantle-derived materials: Nature, v. 569, p. 378–382, https://doi.org/10.1038/s41586-019-1189-0.

Lucey, P.G., 2004, Mineral maps of the Moon: Geophysical Research Letters, v. 31, L08701, https://doi.org/10.1029/2003GL019406.

Lucey, P.G., Taylor, G.J., Hawke, B.R., and Spudis, P.D., 1998, FeO and TiO_2 concentrations in the South Pole–Aitken basin: Implications for mantle composition and basin formation: Journal of Geophysical Research: Planets, v. 103, E2, p. 3701–3708, https://doi.org/10.1029/97JE03146.

Lucey, P.G., Norman, J.A., Crites, S.T., Taylor, G.J., Hawke, B.R., Lemelin, M., and Melosh, H.J., 2014, A large spectral survey of small lunar craters: Implications for the composition of the lunar mantle: The American Mineralogist, v. 99, p. 2251–2257, https://doi.org/10.2138/am-2014-4854.

Melosh, H.J., Kendall, J., Horgan, B., Johnson, B.C., Bowling, T., Lucey, P.G., and Taylor, G.J., 2017, South Pole–Aitken basin ejecta reveal the Moon's upper mantle: Geology, v. 45, p. 1063–1066, https://doi.org/10.1130/G39375.1.

Moriarty, D.P., and Pieters, C.M., 2016, Complexities in pyroxene compositions derived from absorption band centers: Examples from *Apollo* samples, HED meteorites, synthetic pure pyroxenes, and remote sensing data: Meteoritics & Planetary Science, v. 51, p. 207–234, https://doi.org/10.1111/maps.12588.

Moriarty, D.P., and Pieters, C.M., 2018, The character of South Pole–Aitken basin: Patterns of surface and subsurface composition: Journal of Geophysical Research: Planets, v. 123, p. 729–747, https://doi.org/10.1002/2017JE005364.

Moriarty, D.P., Watkins, R.N., Valencia, S.N., Kendall, J.D., and Petro, N.E., 2019, Mineralogy of thorium-enhanced materials within the South Pole–Aitken basin: Possible traces of the lunar upper mantle, *in* 50th Lunar and Planetary Science Conference: Houston, Texas, Lunar and Planetary Institute #2874.

Morrison, D.A., 1998, Did a thick South Pole–Aitken basin melt sheet differentiate to form cumulates?, *in* 29th Lunar and Planetary Science Conference: Houston, Texas, Lunar and Planetary Institute #1657.

Nakamura, R., et al., 2009, Ultramafic impact melt sheet beneath the South Pole-Aitken basin on the Moon: Geophysical Research Letters, v. 36, L22202, https://doi.org/10.1029/2009GL040765.

Ohtake, M., Uemoto, K., Yokota, Y., Morota, T., Yamamoto, S., Nakamura, R., Haruyama, J., Iwata, T., Matsunaga, T., and Ishihara, Y., 2014, Geologic structure generated by large-impact basin formation observed at the South Pole–Aitken basin on the Moon: Geophysical Research Letters, v. 41, p. 2738–2745, https://doi.org/10.1002/2014GL059478.

Pieters, C.M., Fischer, E.M., Rode, O., and Basu, A., 1993, Optical effects of space weathering: The role of the finest fraction: Journal of Geophysical Research: Planets, v. 98, E11, p. 20817–20824, https://doi.org/10.1029/93JE02467.

Pieters, C.M., Taylor, L.A., Noble, S.K., Keller, L.P., Hapke, B., Morris, R.V., Allen, C.C., McKay, D.S., and Wentworth, S., 2000, Space weathering on airless bodies: Resolving a mystery with lunar samples: Meteoritics & Planetary Science, v. 35, p. 1101–1107, https://doi.org/10.1111/j.1945-5100.2000.tb01496.x.

Pieters, C.M., Head, J., Gaddis, L., Jolliff, B., and Duke, M., 2001, Rock types of South Pole–Aitken basin and extent of basaltic volcanism: Journal of Geophysical Research: Planets, v. 106, E11, p. 28001–28022, https://doi.org/10.1029/2000JE001414.

Schultz, P.H., and Gault, D.E., 1985, Clustered impacts: Experiments and implications: Journal of Geophysical Research: Solid Earth, v. 90, B5, p. 3701–3732, https://doi.org/10.1029/JB090iB05p03701.

Shoemaker, E.M., Batson, R.M., Holt, H.E., Morris, E.C., Rennilson, J., and Whitaker, E.A., 1969, Observations of the lunar regolith and the Earth from the television camera on *Surveyor 7*: Journal of Geophysical Research, v. 74, p. 6081–6119, https://doi.org/10.1029/JB074i025p06081.

Vaughan, W.M., and Head, J.W., 2014, Impact melt differentiation in the South Pole–Aitken basin: Some observations and speculations: Planetary and Space Science, v. 91, p. 101–106, https://doi.org/10.1016/j.pss.2013.11.010.

Viviano, C., Murchie, S.L., Daubar, I.J., Morgan, M.F., Seelos, F.P., and Plescia, J.B., 2019, Composition of Amazonian volcanic materials in Tharsis and Elysium, Mars, from MRO/CRISM reflectance spectra: Icarus, v. 328, p. 274–286, https://doi.org/10.1016/j.icarus.2019.03.001.

Wu, W., et al., 2019, Lunar farside to be explored by *Chang'E-4*: Nature Geoscience, v. 12, p. 222–223, https://doi.org/10.1038/s41561-019-0341-7.

Xiao, Z., Zeng, Z., Ding, N., and Molaro, J., 2013, Mass wasting features on the Moon—How active is the lunar surface?: Earth and Planetary Science Letters, v. 376, p. 1–11, https://doi.org/10.1016/j.epsl.2013.06.015.

Yamamoto, S., Nakamura, R., Matsunaga, T., Ogawa, Y., Ishihara, Y., Morota, T., Hirata, N., Ohtake, M., Hiroi, T., and Yokota, Y., 2012, Olivine-rich exposures in the South Pole–Aitken basin: Icarus, v. 218, p. 331–344, https://doi.org/10.1016/j.icarus.2011.12.012.

Zhang, H., Yang, Y., Yuan, Y., Jin, W., Lucey, P.G., Zhu, M.H., Kaydash, V.G., Shkuratov, Y.G., Di, K., and Wan, W., 2015, In situ optical measurements of *Chang'E-3* landing site in Mare Imbrium: 1. Mineral abundances inferred from spectral reflectance: Geophysical Research Letters, v. 42, p. 6945–6950, https://doi.org/10.1002/2015GL065273.

Printed in USA